JOURNAL OF Materials CHEMISTRY

# Oxygen migration in $La_2NiO_{4+\delta}$

**Licia Minervini,[a] Robin W. Grimes,*[a,b] John A. Kilner[a] and Kurt E. Sickafus[b]**

[a]*Department of Materials, Imperial College, London, UK SW7 2BP*
[b]*Los Alamos National Laboratory, Los Alamos, NM 87454, USA*

***Received 26th May 2000, Accepted 10th July 2000***
***First published as an Advanced Article on the web 31st August 2000***

Atomic scale computer simulation based on energy minimization techniques has been used to study excess oxygen accommodation and migration in $La_2NiO_{4+\delta}$. The activation energy for migration in the *ac* plane is predicted to be 0.29 eV, while the activation energy outside the *ac* plane, in the *b* direction is predicted to be 2.90 eV. The activation energies within the *ac* plane are unaffected by the presence of compensating $Ni^{3+}$ defects.



## 1 Introduction

The crystal chemistry underlying the existence of oxygen interstitials in $La_2NiO_{4+\delta}$ is currently of interest due to the high mobility of these defects. Attractive transport properties have led to doped lanthanum nickelates being considered as potential membrane materials in solid state electrochemical devices.[1–3] High oxygen ion mobility is also of significance to solid state catalytic processes and Read *et al.*[4] have conducted preliminary simulations of bulk $La_2NiO_4$, correctly predicting the position of the oxygen interstitial and that the oxidation reaction is exothermic.

Originally, $La_2NiO_{4+\delta}$ was investigated because it is isostructural with the superconducting phase $La_2CuO_{4+\delta}$. In $La_2CuO_{4+\delta}$, holes injected into the $CuO_2$ sheets by the excess oxygen ions make the material superconducting[5,6] and it was hypothesized that if $La_2NiO_{4+\delta}$ behaved similarly, it would also become superconducting.[7–9] Although $La_2NiO_{4+\delta}$ is not a high temperature superconductor,[10] it does accommodate highly mobile excess oxygen up to $\delta = 0.2$. However, the manner in which the holes are accommodated remains unclear, with evidence having been presented for both $O^-$ and $Ni^{3+}$.[11–13]

The aim of the present study is to establish how the excess oxygen is accommodated. Furthermore, we wish to predict the most favourable migration mechanism and pathway for oxygen ions and the associated activation energy.

### 1.1 Crystallography

$La_2NiO_4$ forms as a distorted variant of the tetragonal $K_2NiF_4$ structure, which is closely related to the perovskite structure. The $La_2NiO_4$ structure is formed by stacking alternate rocksalt $La_2O_2$ layers and perovskite $LaNiO_3$ layers (see Fig. 1). However, the ideal tetragonal structure only occurs if the lattice parameters of the two layers match, otherwise a distortion occurs. The mismatch present in $La_2NiO_4$ is minimized through an expansion of the $La_2O_2$ layer, possibly aided by the insertion of oxygen ions, and a compression of the perovskite block through a tilting of the $NiO_6$ octahedra.

The structure of stoichiometric $La_2NiO_4$ at room temperature has been refined in the orthorhombic space group *Cmca* (no. 64).[14–16] We have chosen the standard *Cmca* setting adopted by Kajitani *et al.*[14] rather than the *Bmab* setting adopted by other authors[15,16] (see ref. 17 for more details). The lattice parameters are reported in Table 1 and the atoms occupy the following special positions: La in 8f ($y = 0.3633$, $z = -0.0084$), Ni in 4a, O(1) in 8e ($y = -0.0102$) and O(2) in 8f ($y = 0.1776$, $z = 0.0380$). This structure can accommodate excess lattice oxygen as interstitial defects, O(3), placed at (0.25, 0.25, 0.25).[15] The defect site is located in the $La_2O_2$ rocksalt interlayer and is coordinated tetrahedrally by both $La^{3+}$ and apical oxygen sites (see Fig. 1). Jorgensen *et al.*[15] found that the presence of oxygen interstitial defects forces the apical oxygen ions to be split into two sites, one at the normal O(2) position and the other in a displaced site, O(4), at (−0.06, 0.17, −0.06). The present study successfully predicts the displaced oxygen site to be at (−0.10, 0.17, −0.07).

It is worth noting that this material exhibits a number of different structures, depending on temperatures and small changes in stoichiometry.[16] Calculations will be performed on the stoichiometric $La_2NiO_4$ structure with space group no. 64, which also has the lowest lattice energy. The close lattice energies of the various polymorphs are certainly consistent with their transformation temperatures, although subtle changes in oxygen content may also have a significant influence on the transformations.[16] Table 1 shows that the potential model can reproduce the structures of the various polymorphs and the constituent binary compounds. This is an essential starting point for any reliable computational model.

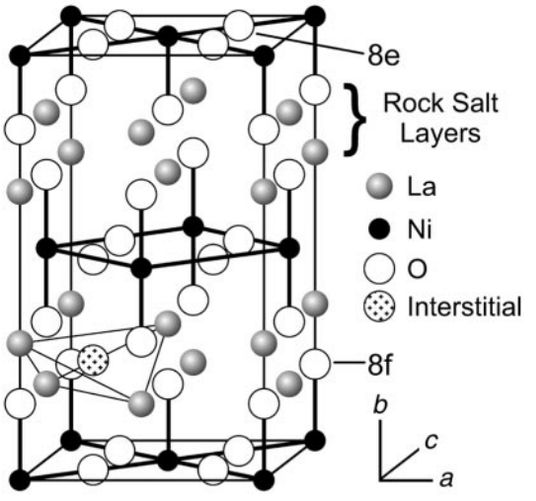


**Fig. 1** The $La_2NiO_4$ unit cell without octahedral canting. The interstitial defect site is shown along with an outline of the tetrahedral La coordination environment. The interstitial site is also tetrahedrally coordinated by apical oxygen ions.

**Table 1** Comparison of predicted and experimental lattice properties

| | | Experimental/Å | | | Predicted deviation (%) | | | | |
|---|---|---|---|---|---|---|---|---|---|
| | Space group | *a* | *b* | *c* | *a* | *b* | *c* | Lattice energy, *U*/eV | Ref. |
| NiO | 225 | 4.0168 | 4.0168 | 4.0168 | −0.53 | −0.53 | −0.53 | −41.34 | 18 |
| $La_2O_3$ | 164 | 3.937 | 4.937 | 6.130 | −0.45 | −0.45 | 1.37 | −127.15 | 19 |
| $La_2NiO_4$ | 139 | 3.855 | 3.855 | 12.652 | −0.85 | −0.85 | 1.71 | −168.22 | 20 |
| $La_2NiO_4$ | 138 | 5.500 | 12.505 | 5.500 | −0.60 | 1.89 | −0.60 | −168.27 | 16 |
| $La_2NiO_4$ | 64 | 5.467 | 12.541 | 5.534 | −1.27 | −0.09 | 1.66 | −168.27 | 14 |

## 2 Methodology

### 2.1 The perfect lattice

Atomistic computer simulation techniques, based on energy minimization with a Born-like description of the lattice,[21] were used to generate the various structures. The procedures are based upon a description of lattice forces in terms of effective potentials. The perfect lattice is described by defining a unit cell which is repeated throughout space using periodic boundary conditions, as defined by the usual crystallographic lattice vectors. The total energy of the crystal is minimized by allowing the ions in the unit cell and the lattice vectors to relax to zero strain. We considered interactions due to long range Coulombic forces, which were summed using Ewald's method,[22] and short range forces that were modeled using parameterized pair potentials, $S_{ij}$. The short range term accounts for the electron cloud overlap and dispersion interactions, which are negligible beyond a few lattice spacings. Thus, in order to reduce the computational time, the short range interactions were set to zero beyond 20 Å. In this study, the Buckingham potential form was used;

$$S_{ij} = A\ e^{(-r_{ij}/\rho)} - C/r_{ij}^6 \quad (1)$$

where $A$, $\rho$ and $C$ are three adjustable parameters (see Table 2).

### 2.2 The defective lattice

In addition to studying the perfect lattice, this approach can be used to predict how the lattice accommodates defects. To do this, the energy-minimized perfect lattice is partitioned into two regions: a spherical inner region, I, at the center of which the defect is introduced, and an outer region, II, which extends to infinity. In region I, interactions are calculated explicitly so that the response of the lattice to the defect is modeled by relaxing the positions of all ions to zero force using a Newton–Raphson minimization procedure.

The response of region II is treated using the Mott–Littleton approximation.[23] To ensure a smooth transition between regions I and II, we have incorporated an interfacial region, IIa, in which ion displacements are determined *via* the Mott–Littleton approximation, but in which interactions with ions in region I are calculated by explicit summation. In the present calculations, the radii of regions I and IIa are approximately 13 and 34 Å, respectively. Region sizes were chosen so as to be large enough to ensure that no appreciable change in defect formation energy occurred if the region sizes were increased further.

**Table 2** Short range potential parameters

| Species | *A*/eV | *ρ*/Å | *C*/eV Å$^6$ |
|---|---|---|---|
| $O^{2-}$–$O^{2-}$ | 9547.96 | 0.2072 | 32.0 |
| $La^{3+}$–$O^{2-}$ | 2119.79 | 0.3459 | 23.25 |
| $Ni^{3+}$–$O^{2-}$ | 1279.23 | 0.2932 | 0.0 |
| $Ni^{2+}$–$O^{2-}$ | 905.40 | 0.3145 | 0.0 |
| $O^-$–$O^-$ | 38 671.37 | 0.1376 | 13.72 |
| $O^{2-}$–$O^-$ | 38 671.37 | 0.1376 | 21.23 |
| $La^{3+}$–$O^-$ | 1764.93 | 0.2724 | 18.26 |
| $Ni^{3+}$–$O^-$ | 1104.29 | 0.2062 | 0.0 |
| $Ni^{2+}$–$O^-$ | 713.65 | 0.2207 | 0.0 |

The polarizability of the ions may be accounted for *via* the shell model originally described by Dick and Overhauser.[24] This consists of a massless shell with charge $Y|e|$ that is allowed to move with respect to a massive core of charge $X|e|$; the overall charge state of each ion is therefore equal to $(X+Y)|e|$. The core and shell charges are connected by an isotropic harmonic spring of force constant $k$. Displacement of the shell relative to the core gives a good description of electronic polarization. In all calculations, $O^{2-}$ is treated as polarizable using the shell model: $Y=-2.04$, $k=6.3$ eV Å$^{-2}$.[25]

The type of calculation employed here is usually referred to as "static", since lattice vibration entropy contributions are not included in the model. Furthermore, configurational entropy is also ignored and the effective positions of ions in the outer region II are held fixed. The energies calculated are therefore changes in the internal energy of the system and relate, *via* the quasi-harmonic approximation, to the temperature of the lattice to which the potential parameters were fitted; in this case, room temperature. For solids, changes in internal energy are generally very similar to changes in enthalpy.[26] Entropy contributions are usually small at room temperature, but, nevertheless, this introduces some uncertainty into any analysis that relies on enthalpies as the sole basis for determining defect structures. For further details of the computational methods, see ref. 27 and 28. In all cases, calculations were carried out using the CASCADE code.[29]

### 2.3 Migration calculations

To establish the most favourable migration pathways, it is necessary to calculate activation energies for each migration path. This is defined as the difference between the energy of the defect at the saddle point and the energy of the defect at equilibrium. The saddle point energy is calculated by introducing a fixed defect at the saddle point location and then relaxing the surrounding lattice. The configuration of the saddle point can be identified by evaluating the potential energy surface both parallel and perpendicular to the diffusion path.

### 2.4 Defect clustering

In this study, defects are treated in two different ways. First, they are assumed to be spatially isolated from each other. The energy of a defect process is then determined by summing the individual energies of each component defect participating in the overall defect reaction. However, since defects in ionic materials are often charged there will be a mutual Coulombic attraction between them. Consequently, when there is sufficient concentration, defect clusters will be formed. Under these circumstances, the energy of the defect reaction is determined by calculating the energy of the complete defect cluster.

### 2.5 Derivation of potential parameters

The values of the potential parameters were chosen to reproduce the unit cell dimensions of the various polymorphs of $La_2NiO_4$ and of the constituent binary oxides (see Table 1). By fitting to a variety of structures, the potentials reflect the

metal–oxygen and oxygen–oxygen interactions over a wider range of inter-atomic separations than would be the case if the fitting process were restricted to a single structure. This is significant, since we shall be concerned with defects and the ions surrounding the defect will relax away from their equilibrium positions.

Due to the lack of experimental data, potential parameters involving $O^-$ and $Ni^{3+}$ species were initially obtained using the electron gas techniques of Wedepohl[30] and Gordon and Kim.[31] These starting parameters were then empiricized to achieve a consistent set of potentials.[32] Finally, the lattice volume of $La_2NiO_{4+\delta}$ as a function of $\delta$, reported by Rice and Buttrey,[33] was used as a means to empirically fit $O^-$ and $Ni^{3+}$ potentials. Oxygen interstitial ions were introduced into a $2a \times 2b \times 2c$ large unit cell (where $a$, $b$ and $c$ are the lattice parameters of $La_2NiO_4$) to simulate non-stoichiometry. Charge neutrality was maintained in the lattice by introducing either lattice $O^-$ or $Ni^{3+}$ ions. The potential parameters for interactions involving $O^-$ and $Ni^{3+}$ species were then adjusted to best reproduce the observed lattice volume variation. We shall return to this issue at the end of section 3.2.

## 3 Results and discussion

### 3.1 Intrinsic defects

The results are collected in Table 3. Anion Frenkel pairs, composed of a vacancy on the 8e site and an interstitial at (0.25, 0.25, 0.25), are predicted to be the dominant type of lattice disorder; similar results have been obtained for the isomorphous $A_2CuO_4$ (A = La, Nd) compounds by Allan and Mackrodt.[34,35] As previously shown by Allan *et al.*,[36] oxygen vacancies at the equatorial sites (8e) in the $NiO_2$ planes are found to be more energetically favourable than those in apical sites (8f).

### 3.2 Excess oxygen

It is known that $La_2NiO_{4+\delta}$ undergoes an oxidation process whereby additional oxygen ions are accommodated interstitially in the lattice. Excess oxygen ions can potentially be compensated for *via* several mechanisms, involving either cation antisite, oxygen vacancies, oxidized lattice oxygen ions or oxidized nickel ions. Defect energy calculations involving the latter species (*i.e.* $O^-$ and $Ni^{3+}$) are more difficult than those involving only structural defects. Difficulties arise because: (i) the holes may not be completely localized on individual ions as we are forced to assume, (ii) since the $O^{2-}$ ions are only stable against dissociation when confined within a Madelung potential well,[37] their properties depend to some extent on the crystallography (however, here we are able to calculate this value from thermodynamic data—see Appendix A) and (iii) in the case of $Ni^{3+}$, we have to include a contribution due to the crystal field splitting of the d orbitals (here, we are able to calculate this value from spectroscopic data—see Appendix B).

The reactions considered in this study and the relative reaction energies are summarized in Table 4. The $O_2$ dissociation energy is 5.116 eV,[38] the first electron affinity of oxygen is −1.461 eV,[38] the second electron affinity of oxygen, calculated using a Born–Haber cycle,[39] is 8.0 eV (see Appendix A) and the third ionization energy of Ni is 34.41 eV,[38] which includes an octahedral site crystal field correction of −0.78 eV to form low spin $Ni^{3+}$ [40,41] (see Appendix B). The most favourable reactions are those where an interstitial oxygen ion is compensated for, either by oxidized nickel ions, or by a combination of both an oxidized lattice oxygen ion and an oxidized nickel ion.

These results (see Table 4) suggest that when defects are isolated, true for very small values of $\delta$ in $La_2NiO_{4+\delta}$, the charge compensating holes will reside on nickel sites, *i.e.* reactions F and G exhibit the lowest energies. At larger values of $\delta$, when defect clustering becomes more likely, holes may

**Table 3** Intrinsic disorder defect energies for $La_2NiO_4$

| Disorder mechanism | | Defect energy/eV defect$^{-1}$ |
|---|---|---|
| Schottky | $2V'_{La} + V''_{Ni} + 4V^{\bullet\bullet}_{O(8e)} + La_2NiO_4\uparrow$ | 3.02 |
| $La_2O_3$ partial Schottky | $2V'_{La} + 3V^{\bullet\bullet}_{O(8e)} + La_2O_3\uparrow$ | 2.74 |
| NiO partial Schottky | $V''_{Ni} + V^{\bullet\bullet}_{O(8e)} + NiO\uparrow$ | 3.23 |
| $La^{3+}$ Frenkel | $V'_{La} + La^{\bullet\bullet\bullet}_{i(8c)}$ | 7.08 |
| $Ni^{2+}$ Frenkel | $V''_{Ni} + Ni^{\bullet\bullet}_{i(8c)}$ | 4.62 |
| $O^{2-}$ Frenkel | $V^{\bullet\bullet}_{O(8e)} + O''_i$ | 2.27 |
| $O^{2-}$ Frenkel | $V^{\bullet\bullet}_{O(8f)} + O''_i$ | 2.59 |
| Cation antisite | $La^{\bullet}_{Ni} + Ni'_{La}$ | 3.26 |

**Table 4** Oxygen excess compensation mechanisms

| | | Energy/eV | |
|---|---|---|---|
| | Compensation mechanism | Isolated defects | Clustered defects |
| A | $3La_2O_3 \rightarrow 2La^{\bullet}_{Ni} + O''_i + 4La^{\times}_{La} + 8O^{\times}_O$ | 11.44 | 7.89 |
| B | $3La_2O_3 + 1/2O_2 \rightarrow 2La^{\bullet}_{Ni} + 2O'_i + 4La^{\times}_{La} + 8O^{\times}_O$ | 4.93 | 4.08 |
| C | $1/2O_2 + O^{\times}_O \rightarrow 2O'_i + V^{\bullet\bullet}_O$ | −1.96 | — |
| D | $1/2O_2 + O^{\times}_O \rightarrow O'_i + O^{\bullet}_O$ | −3.99 | −5.00 |
| E | $1/2O_2 + 2O^{\times}_O \rightarrow O'_i + 2O^{\bullet}_O$ | −1.48 | −6.28 |
| F | $1/2O_2 + Ni^{\times}_{Ni} \rightarrow O'_i + Ni^{\bullet}_{Ni}$ | −6.57 | −6.87 |
| G | $1/2O_2 + 2Ni^{\times}_{Ni} \rightarrow O''_i + 2Ni^{\bullet}_{Ni}$ | −6.63 | −7.56 |
| H | $1/2O_2 + Ni^{\times}_{Ni} + O^{\times}_O \rightarrow O''_i + Ni^{\bullet}_{Ni} + O^{\bullet}_O$ | −3.58 | −7.92 |

reside on a mixture of both nickel and oxygen sites, *i.e.* reactions G and H are lowest. In all such cases, the holes will be in the NiO planes rather than the $La_2O_2$ planes and the oxygen interstitial ions may be either $O^-$ or $O^{2-}$. However, given some uncertainty introduced by variables such as the second electron affinity of oxygen, we cannot confidently discern between reactions G and H, and even reaction F could remain of significance at higher concentrations. In this regard there are also conflicting experimental studies. For example, the existence of $O_2^{2-}$ species as defects has been corroborated by Buttery *et al.*,[12] while other results suggest that nickel exists in a mixed valence state and is the predominant charge compensating defect.[4,11,13] This disagreement may be due to differences in the value of $\delta$. Nevertheless, whatever the eventual consensus, our predictions clearly agree that the oxidation process is exothermic.[13]

The predicted lattice volume of $La_2NiO_{4+\delta}$ as a function of $\delta$ also has a bearing on this issue. As stated in section 2.5, the potentials associated with $O^-$ and $Ni^{3+}$ were empiricized[32] to best reproduce the experimental variation. The results of this process are presented in Table 5, which compares the experimental variation in lattice volume as a function of $\delta$ to the variation predicted for the various charge compensating mechanisms calculated using the large unit cell approach. The experimental variation appears to be linear up to $\delta = 0.05$.[12] Clearly, the models which include some participation from $Ni^{3+}$ are far more successful in reproducing experiment than models which assume only $O^-$. This suggests that the reduction in lattice volume upon incorporation of oxygen is a consequence of the formation of low spin $Ni^{3+}$.

### 3.3 Oxygen migration

Migration of oxygen ions in the oxygen excess material was found to occur *via* an intersticialcy mechanism. Resulting migration energies within the *ac* plane and in the *b* direction are reported in Table 6. In both cases, movement of $O^{2-}$ and $O^-$ interstitial ions was considered. The effect of neighbouring $Ni^{3+}$ was also taken into consideration. Migration within the *ac* plane occurs with a far lower activation energy than migration in the *b* direction, implying that migration will be highly anisotropic. Furthermore, oxygen migration is largely unaffected by the presence of neighbouring $Ni^{3+}$ ions within the *ac* plane. This implies that migration may not be greatly influenced by the presence of defects or possibly even impurities.

The migration mechanism within the *ac* plane involves oxygen interstitial ions moving into apical oxygen sites (8f), which in turn become interstitial ions (see Fig. 2, mechanism a). This would cause the migrating species to alternate between $O^{2-}$ and $O^-$, even though the transport of an $O^-$ is more energetically favourable. However, eqn. 2 shows that charge transfer will readily occur.

$$(O''_i : O_O^\bullet)' \rightarrow O'_i + O_O^\times \quad \Delta E = 0.01 \text{ eV} \qquad (2)$$

Thus, oxygen migrates as $O^-$, then, as it approaches the lattice

**Table 5** Comparison of experimental and predicted lattice volume variation with non-stoichiometry at $\delta = 0.05$ ($\Delta V/V_o$)

| Defects | $\Delta V/V_o$ (%) |
|---|---|
| Experiment[33] | −0.28 |
| $O'_i + O_O^\bullet$ | 0.08 |
| $O''_i + 2O_O^\bullet$ | 0.40 |
| $O'_i + Ni_{Ni}^\bullet$ | −0.21 |
| $O''_i + 2Ni_{Ni}^\bullet$ | −0.28 |
| $O''_i + Ni_{Ni}^\bullet + O_O^\bullet$ | −0.33 |

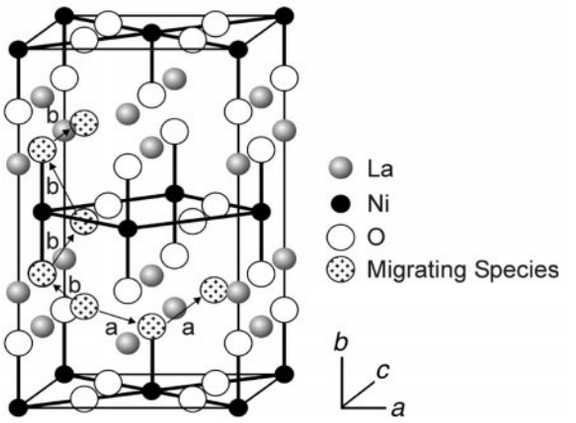


**Fig. 2** Mechanisms for (a) *ac* plane and (b) *b* direction migration.

site, charge transfer occurs so that the lattice ion remains $O^{2-}$ and the migrating species remains $O^-$. Migration in the *b* direction also occurs *via* an intersticialcy mechanism, as shown in Fig. 2, mechanism b. Although the presence of $Ni^{3+}$ in the vicinity of oxygen interstitial species is of little consequence for migration within the *ac* plane, this is not the case for migration in the *b* direction. This is probably due to the fact that when oxygen migrates through the *ac* plane, $Ni^{3+}$ ions can remain associated to the interstitial species by migrating within a NiO plane rather than through a $La_2O_2$ plane. When the oxygen ion migrates in the *b* direction, the associated $Ni^{3+}$ ion must either become unassociated with the migrating oxygen or the hole must migrate through a $La_2O_2$ plane. This factor increases the predicted anisotropy in the activation energy for migration. Anisotropy in and out of the *ac* plane (*i.e.* the rocksalt layers) was also predicted by Allan and Mackrodt in $La_2CuO_4$.[42]

In a recent study, Skinner and Kilner[1] measured the activation energy for diffusion in $La_2NiO_{4+\delta}$ ($\delta = 0.24$) as 0.85 eV. Since the samples measured were polycrystalline, this value represents a compromise between *ac* and *b* directions and, therefore, falls between the values that we predict for migration in the *ac* plane and the *b* direction. Nevertheless, even in the polycrystalline state, the oxygen transport properties of $La_2NiO_{4+\delta}$ were found to be almost as good as current acceptor-doped perovskite mixed ionic electronic conductors, such as $La_{0.3}Sr_{0.7}CoO_{3-\delta}$ (LSC) and $La_{1-x}Sr_xCo_{1-y}Fe_yO_{3-\delta}$ (LSCF). Oxygen tracer diffusion studies in isostructural $La_{1.9}Sr_{0.1}CuO_{4-y}$[43] indicate that the activation energy for diffusion in the *b* direction is 1.31 eV, while that for polycrystalline samples of the same composition ranges from 0.65 to 0.80 eV. If it is assumed that diffusion in the polycrystalline sample occurs primarily along the *ac* planes, then there is considerable diffusion anisotropy in this material. Thus, if anisotropy is as marked as we predict, migration would be greatly enhanced if textured layers could be formed for device applications.

## 4 Conclusions

Atomistic simulation calculations have been shown to reproduce the various $La_2NiO_4$ polymorphs and the position

**Table 6** Oxygen ion migration energies. Values in parentheses incorporate the compensating Ni defects in the migration process

| | Energy/eV | |
|---|---|---|
| Migrating species | *ac* plane | *b* direction |
| $O'_i$ | 0.29 (0.29) | 2.90 (3.25) |
| $O''_i$ | 0.88 (0.88) | 3.15 (3.46) |

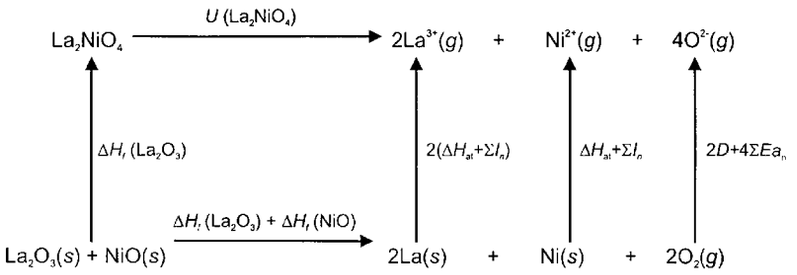


**Fig. 3** Born–Haber cycle for the formation of $La_2NiO_4$ from its component oxides, where $\Delta H_f$ is the enthalpy of formation, $\Delta H_{at}$ and $D$ are the enthalpies of atomization of the cation and oxygen, respectively, $I_n$ is the $n$th ionization energy of the cation and $E_{a_n}$ is the $n$th electron affinity of oxygen.

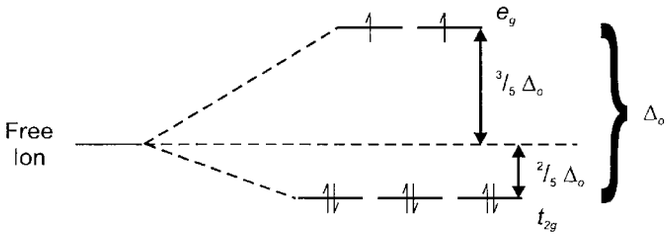


**Fig. 4.** Splitting of the ground state five d orbitals of a $Na^{2+}$ ion by an octahedral field.

of the split apical oxygen ion. Consequently, defect formation and migration can be investigated, contributing to the understanding of this potential cathode material for the next generation of fuel cells. In particular, this work has highlighted the following features:

(1) An anion Frenkel pair, composed of a vacancy on the 8e site and an interstitial at (0.25, 0.25, 0.25), provides the lowest energy intrinsic disorder process.
(2) An excess oxygen ion is incorporated into the lattice as an interstitial $O^{2-}$ or $O^-$ ion that can be compensated for by $Ni^{3+}$ ions or by a combination of an $O^-$ and a $Ni^{3+}$ ion.
(3) Oxygen ion migration is highly anisotropic and, within the *ac* plane, relatively independent of surrounding $Ni^{3+}$ cation defects. This has obvious significance for device fabrication.

## Acknowledgements

Support for this work was provided by the Department of Energy, Office of Basic Sciences, Division of Materials Sciences. Some computing facilities were provided by EPSRC grant number GR/L86821.

**Table 7** Component energies for the Born–Haber cycle, where $\Delta H_f$ is the enthalpy of formation, $\Delta H_{at}$ and $D$ are the enthalpies of atomization of the cation and oxygen, respectively, $I_n$ is the $n$th ionization energy of the cation and $E_{a_n}$ is the $n$th electron affinity of oxygen. In all cases, the subscript ∞ implies that the ion is in a state of rest at infinity, *i.e.* removed from interaction with any other matter

| Reaction | Energy | eV | Reference |
|---|---|---|---|
| $La_2O_3+NiO \rightarrow La_2NiO_4$ | $\Delta H_{f(La_2NiO_4)}$ | 0.27 | 45 |
| $2La_s+3/2(O_2) \rightarrow La_2O_3$ | $\Delta H_{f(La_2O_3)}$ | −18.59 | 46 |
| $Ni_s+1/2(O_2) \rightarrow NiO$ | $\Delta H_{f(NiO)}$ | −2.49 | 46 |
| $La_s \rightarrow La_g$ | $\Delta H_{at(La)}$ | 4.47 | 47 |
| $Ni_s \rightarrow Ni_g$ | $\Delta H_{at(Ni)}$ | 4.45 | 47 |
| $(O_2)_\infty \rightarrow 2O_\infty$ | $D$ | 5.116 | 38 |
| $O_\infty+e^-_\infty \rightarrow O^-_\infty$ | $E_{a_1}$ | −1.46 | 38 |
| $La_\infty \rightarrow La^{1+}_\infty+e^-_\infty$ | $I_{1(La)}$ | 5.58 | 38 |
| $La^{1+}_\infty \rightarrow La^{2+}_\infty+e^-_\infty$ | $I_{2(La)}$ | 11.06 | 38 |
| $La^{2+}_\infty \rightarrow La^{3+}_\infty+e^-_\infty$ | $I_{3(La)}$ | 19.18 | 38 |
| $Ni_\infty \rightarrow Ni^{1+}_\infty+e^-_\infty$ | $I_{1(Ni)}$ | 7.64 | 38 |
| $Ni^{1+}_\infty \rightarrow Ni^{2+}_\infty+e^-_\infty$ | $I_{2(Ni)}$ | 18.17 | 38 |

# Appendix

## A Second electron affinity of oxygen

In free space, $O^-$ is stable but $O^{2-}$ is not, the latter only becomes stable within a crystal. In the crystal, $O^{2-}$ is stabilized because it sits in a deep potential well created by the other ions of the structure (largely the Madelung potential well) (see, for example, ref. 28 and 44). Consequently the electronic contribution of the energy required to reduce $O^-$ to $O^{2-}$, known as the second electron affinity, is a positive quantity, *i.e.* work must be done to create $O^{2-}_\infty$ from $O^-_\infty$ plus an electron. Since $O^{2-}$ is only stable in the crystal, its properties, in particular the second electron affinity, would be expected to depend on the crystal environment. It follows, therefore, that the common practice of using an average value of the second electron affinity obtained by applying the Born–Haber cycle[39] to one series of like compounds when making calculations for other compounds is basically inconsistent. This may become particularly significant when trying to model changes in stoichiometry.

Here, due to the availability of appropriate thermodynamic data, we have used the Born–Haber cycle to determine the specific second electron affinity for oxygen in $La_2NiO_4$. The Born–Haber cycle in principle uses thermodynamic enthalpy data referred to standard conditions. However, adjustments of measured or calculated quantities (such as lattice energies) appropriate to other temperatures, being of the order of $R(T-298)$ per mole, are generally negligible in comparison with the second affinity and are no greater than the uncertainties in the calculated lattice energies. Also, the differences between the thermodynamic internal energies and the corresponding enthalpies are of the same order for the gaseous phase and much smaller for solid phases. These corrections are, therefore, not taken into account. With the aid of the data in Table 7 and the calculated lattice energy of $La_2NiO_4$, $U_{(La_2NiO_4)}$ (Table 1), we have obtained a value of 8.0 eV for the second electron affinity of oxygen in $La_2NiO_4$ from the Born–Haber cycle shown in Fig. 3. The enthalpy of formation for $La_2NiO_4$ was extracted from the Gibbs free energy of formation at elevated temperature (1123–1373 K) determined by Sreedharan and Pankajavalli.[45] DiCarlo *et al.*[13] found that the enthalpy of formation for $La_2NiO_4$ is very close

to zero ($0.02 \pm 0.05$ eV), this value will, nonetheless, also yield a second electron affinity of 8.0 eV.

## Appendix

## B Crystal field correction

When isolated, a gaseous $Ni^{3+}$ ion does not experience an electrostatic field and the five d orbitals are degenerate. However, in a crystal, the symmetry of the field is less than spherical and the degeneracy is removed. In $La_2NiO_4$, Ni is in an octahedral environment so that the d orbitals are split into 2 sets, a lower energy set ($t_{2g}$) consisting of three orbitals and a higher energy set ($e_g$) consisting of 2 orbitals (see Fig. 4). Therefore, a correction term from the splitting of the d orbitals by the crystal field must be incorporated into the third ionization energy of nickel. Due to the low spin nature of $Ni^{3+}$ [48,49] we assume that in ionizing $Ni^{2+}$ the electron is removed from an $e_g$ orbital and the ionization energy of $Ni^{2+}$ is lowered by $3/5\Delta_o = 0.78$ eV (see Fig. 4).[40,41]

## References


1 S. J. Skinner and J. A. Kilner, *Solid State Ionics*, 2000, in press.
2 Norsk Hydryo ASA, *A Membrane and Use Thereof*, International Patent, PCT/NO98/00172, 1999.
3 V. V. Kharton, A. P. Viskup, E. N. Naumovich and F. M. B. Marques, *J. Mater. Chem.*, 1999, **9**, 2623.
4 M. S. D. Read, M. S. Islam, F. King and F. E. Hancock, *J. Phys. Chem. B*, 1999, **103**, 1558.
5 J. Beille, R. Cabanel, G. Chaillout, B. Chevalier, G. Demazeau, F. Deslandes, J. Etourneau, P. Lejay, C. Michel, J. Provost, B. Raveau, A. Sulpice, J. L. Tholence and R. Tounier, *C.R. Acad. Sci., Ser. II*, 1987, **304**, 1097.
6 J. D. Jorgensen, B. Dabrowski, S. Pei, D. G. Hinks, L. Soderholm, B. Morosin, J. E. Schirber, E. L. Venturini and D. S. Ginley, *Phys. Rev. B: Condens. Matter*, 1988, **38**, 11337.
7 Z. Kakol, J. Spalek and J. M. Honig, *Solid State Commun.*, 1989, **71**, 283.
8 Z. Kakol, J. Spalek and J. M. Honig, *Solid State Commun.*, 1989, **71**, 511.
9 Z. Kakol, J. Spalek and J. M. Honig, *Solid State Commun.*, 1989, **79**, 288.
10 S. A. Hoffman, C. Venkatraman, S. N. Ehrlich, S. M. Durbin and G. L. Liedl, *Phys. Rev. B: Condens. Matter*, 1991, **43**, 7852.
11 R. Sáez Puche, J. L. Rodriguez and F. Fernández, *Inorg. Chim. Acta*, 1987, **140**, 151.
12 D. J. Buttrey, P. Ganguly, J. M. Honig, C. N. Rao, R. R. Schartman and G. N. Subbanna, *J. Solid State Chem.*, 1988, **74**, 233.
13 J. DiCarlo, A. Metha, D. Banschick and A. Navrotsky, *J. Solid State Chem.*, 1993, **103**, 186.
14 T. Kajitani, Y. Kitagaki, K. Hiraga, S. Hosoya, T. Fukuda, Y. Yamaguchi, S. Wada, S. Sugai, Y. Morii, K. Fuchizaki and S. Funahashi, *Physica C*, 1991, **185**, 579.
15 J. D. Jorgensen, B. Dabrowski, S. Pei, D. R. Richards and D. G. Hinks, *Phys. Rev. B: Condens. Matter*, 1989, **40**, 2187.
16 J. Rodríguez-Carvajal, M. T. Fernàndez-Díaz and J. L. Martínez, *J. Phys.: Condens. Matter*, 1991, **3**, 3215.
17 In the *Cmca* setting, the long axis of the orthorhombic unit cell lies along the *b* direction, while in the *Bmab* setting, it lies along the *c* direction.
18 R. W. G. Wyckoff, *Crystal Structures*, 2nd edn., John Wiley & Sons, Inc., New York, 1963, vol. 1.
19 R. W. G. Wyckoff, *Crystal Structures*, 2nd edn., John Wiley & Sons, Inc., New York, 1964, vol. 2.
20 R. W. G. Wyckoff, *Crystal Structures*, 2nd edn., John Wiley & Sons, Inc., New York, 1965, vol. 3.
21 M. Born, *Atomtheorie des Festen Zustandes*, Teubner, Leipzig, 1923.
22 P. P. Ewald, *Ann Phys. (Leipzig)*, 1921, **64**, 253.
23 N. F. Mott and M. J. Littleton, *Trans. Faraday Soc.*, 1932, **34**, 485.
24 B. G. Dick and A. W. Overhauser, *Phys. Rev.*, 1958, **112**, 90.
25 R. W. Grimes, G. Busker, M. A. McCoy, A. Chroneos and J. A. Kilner, *Ber. Bunsen-Ges. Phys. Chem.*, 1997, **101**, 1204.
26 E. B. Smith, *Basic Chemical Thermodynamics*, 3rd edn., Oxford University Press, Oxford, 1983.
27 *Computer Simulation of Solids*, ed. C. R. A. Catlow and W. C. Mackrodt, Springer-Verlag, Berlin, 1982.
28 A. H. Harker and R. W. Grimes, *The Practical Calculation of Interionic Potentials in Solids*, in special issues of *Mol. Simul.* **4**(5) and **5**(2), Gordon and Breach Publishing Group, New York, 1990.
29 M. Leslie, DL/SCI/TM31T, Technical report, SERC Daresbury Laboratory, 1982.
30 P. T. Wedepohl, *Proc. Phys. Soc.*, 1967, **92**, 79.
31 R. G. Gordon and Y. S. Kim, *J. Chem. Phys.*, 1972, **56**, 3122.
32 R. W. Grimes, C. R. A. Catlow and A. M. Stoneham, *J. Phys.: Condens. Matter*, 1989, **1**, 7367.
33 D. E. Rice and D. J. Buttrey, *J. Solid State Chem.*, 1993, **105**, 197.
34 N. L. Allan and W. C. Mackrodt, *J. Am. Ceram. Soc.*, 1990, **73**, 3175.
35 N. L. Allan and W. C. Mackrodt, *Mol. Simul.*, 1994, **12**, 89.
36 N. L. Allan, J. M. Lawton and W. C. Mackrodt, *Philos. Mag. B*, 1989, **59**, 191.
37 R. W. Grimes, *Mol. Simul.*, 1990, **5**, 9.
38 *CRC Handbook of Chemistry and Physics*, 78th edn., ed. D. R. Lide, CRC Press, Inc., Boca Raton, FL, 1997–1998.
39 T. C. Waddington, *Adv. Inorg. Chem. Radiochem.*, 1959, **1**, 157.
40 D. Ž. Obadović, J. Kiurski and R. Marinković-Nedučin, *Polyhedron*, 1996, **15**, 3631.
41 G. van der Laan, C. M. B. Henderson, R. A. D. Patrick, S. S. Dhesi, P. F. Scofield, E. Dudzik and D. J. Vaughn, *Phys. Rev. B: Condens. Matter*, 1999, **59**, 4314.
42 N. L. Allan and W. C. Mackrodt, *Philos. Mag. A*, 1991, **64**, 1129.
43 E. J. Opila, H. L. Tuller and B. J. Wuensch, *J. Am. Ceram. Soc.*, 1993, **76**, 2363.
44 W. C. Mackrodt and R. F. Stewart, *J. Phys. C: Solid State Phys.*, 1979, **12**, 5015.
45 O. M. Sreedharan and R. Pankajavalli, *J. Mater. Sci. Lett.*, 1984, **3**, 388.
46 O. Kubaschewski and C. B. Alcock, *Metallurgical Thermochemistry*, 5th edn., Pergamon Press, Oxford, 1979.
47 A. M. James and M. P. Lord, *Macmillan's Chemical and Physical Data*, Macmillan, London, 1992.
48 J. B. Goodenough, N. F. Mott, M. Pouchard and G. Demazeau, *Mater. Res. Bull.*, 1973, **8**, 647.
49 T. A. Ivanova, Y. V Yablokov, N. S. Zinatullina and R. M. Bayazitov, *Sov. Phys. Solid State (Engl. Transl.)*, 1999, **41**, 375.